Estimates of the 10-m Neutral Sea Surface Drag Coefficient from Aircraft Eddy-Covariance Measurements

DEAN VICKERS

Oregon State University, Corvallis, Oregon

LARRY MAHRT

Northwest Research Associates (Seattle Division), Corvallis, Oregon

EDGAR L ANDREAS

Northwest Research Associates (Seattle Division), Lebanon, New Hampshire

(Manuscript received 8 June 2012, in final form 18 September 2012)

ABSTRACT

The 10-m neutral drag coefficient (C_{DN10}) over the sea is calculated using a large observational dataset consisting of 5800 estimates of the mean flow and the fluxes from aircraft eddy-covariance measurements. The dataset includes observations from 11 different experiments with four different research aircraft. One of the goals is to investigate how sensitive C_{DN10} is to the analysis method. As such, C_{DN10} derived from six unique processing schemes that involve different methods for averaging the surface stress and the wind speed are compared. Especially in weak winds, the resulting C_{DN10} values depend on the choice of processing.

Four distinct regimes of C_{DN10} are identified: weak winds where calculating C_{DN10} is not well posed, moderate winds (4 to 10 m s^{-1}) where C_{DN10} is a constant, strong winds (10 to 20 m s^{-1}) where C_{DN10} increases linearly with increasing wind speed, and very strong winds (20 to 24 m s^{-1}) where C_{DN10} steadily decreases with increasing wind speed. However, as this last regime is based on data from a single experiment, additional data are needed to confirm this apparent decrease in C_{DN10} for winds exceeding 20 m s^{-1}.

1. Introduction

A large aircraft dataset of eddy-covariance turbulence flux measurements over the sea is used to examine the dependence of the drag coefficient on wind speed. We obtained the raw fast-response data for 11 different experiments from 1992 to 2008 with four different aircraft. The observed wind and eddy-covariance fluxes from low-level flight segments are combined with Monin–Obukhov similarity theory and standard stability functions to calculate the 10-m neutral equivalent wind speed and the 10-m neutral drag coefficient. The traditional reduction to the 10-m neutral coefficient is somewhat unsatisfying because of uncertainty in the stability functions, the assumption that conditions do not violate the requirements for Monin–Obukhov similarity theory, and the influence of unknown wave-state effects; however, there are no other well established alternatives.

We will explore the effects of the reduction to 10-m neutral for these data. Estimates of the 10-m neutral drag coefficient are compared to the Charnock formulation (Charnock 1955) used in the Tropical Ocean and Global Atmosphere Coupled Ocean–Atmosphere Response Experiment (TOGA COARE) bulk flux algorithm (Fairall et al. 1996, 2003), a consensus formulation published by Garratt (1977) based on an extensive literature review, the formulation of Large and Pond (1981), and to other published estimates (Fig. 1).

Uncertainty in predicting the stress in weak winds may be associated with differences between the stress vector and mean wind and surface wave directions (Rieder et al. 1994; Grachev et al. 2003). For example, if the weak wind cases are primarily wind opposing swell, we might expect the drag coefficient to be larger than the Charnock plus smooth flow formulation, which does not

Corresponding author address: Dean Vickers, Oregon State University, College of Earth, Ocean and Atmospheric Sciences, CEOAS Admin Bldg. 104, Corvallis, OR 97331.
E-mail: vickers@coas.oregonstate.edu

DOI: 10.1175/JPO-D-12-0101.1

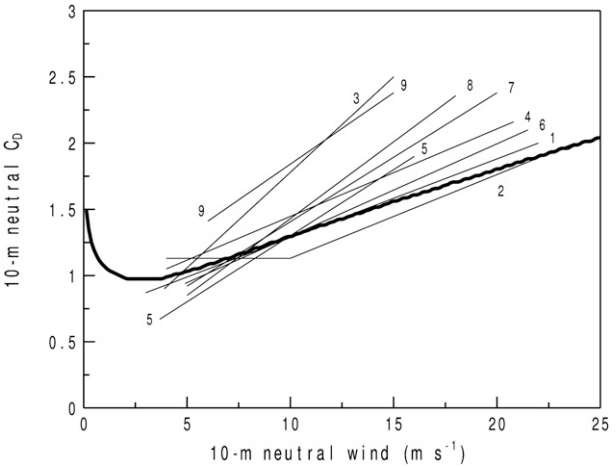

FIG. 1. Published drag coefficient wind speed relationships: 1) Smith (1980), 2) Large and Pond (1981), 3) Donelan (1982), 4) Garratt (1977), 5) Sheppard et al. (1972), 6) Smith and Banke (1975), 7) Geernaert et al. (1986), 8) Smith et al. (1992), 9) Smith et al. (1992) ''very young waves.'' The heavy curve is the Charnock plus smooth flow relationship with $\alpha = 0.011$. The drag coefficient has been multiplied by 10^3 to make it of order one.

include this effect. In addition, we will explore the uncertainty of the fluxes in weak winds due to the choice of analysis methods.

The large uncertainty in the neutral drag coefficient for strong winds is related to a lack of measurements owing to the obvious difficulties obtaining aircraft or ship-based turbulence measurements in gale force winds. In the widely used TOGA COARE bulk flux algorithm (Fairall et al. 2003), the authors caution that their surface stress algorithm is not valid for winds exceeding 20 m s^{-1}. The generality of our results for very strong winds is limited because only one experiment, of the 11 where we could obtain the raw data, has wind speeds exceeding 20 m s^{-1}, and there are no observations with speeds exceeding 30 m s^{-1}.

2. Aircraft data

A large dataset is used in this study (Table 1). We analyze raw (fast-response) data collected by the National Oceanic and Atmospheric Administration (NOAA) Long-EZ aircraft during four experiments: 1) the pilot program of the Coupled Boundary Layers and Air Sea Transfer experiment (CBLAST Weak Wind) conducted over the Atlantic Ocean south of Martha's Vineyard Island, MA, during July–August 2001 (Edson et al. 2007); 2) the Shoaling Waves experiment (SHOWEX) during November and December 1999 over the Atlantic east of the Outer Banks near Duck, NC (Sun et al. 2001); 3) the SHOWEX pilot study in November 1997; and 4) the SHOWEX pilot study in March 1999.

TABLE 1. The 11 aircraft datasets where we processed the fast-response data, computed the fluxes, and performed the reduction to 10-m neutral. The N is the number of 4-km data points, z is the range of heights of the measurements, U is the observed mean wind speed at height z averaged over the entire experiment, and Max U is the maximum 4-km wind speed at height z. The total number of 4-km data points is 6125.

Dataset	N	z (m)	U (m s^{-1})	Max U (m s^{-1})
Long-EZ SHOWEX Nov 97	508	10–49	6.5	12.0
Long-EZ SHOWEX Mar 99	199	10–48	10.0	17.3
Long-EZ SHOWEX Nov 99	970	10–48	5.9	16.5
Long-EZ CBLAST Jul–Aug 01	740	10–16	5.3	9.2
Twin Otter CARMA IV Aug 07	650	27–40	7.3	18.0
Twin Otter Monterey Apr 08	654	26–39	11.2	18.1
Twin Otter RED Aug–Sep 01	373	23–49	7.9	17.9
Twin Otter MABLEB Apr 07	45	29–38	10.1	18.0
Twin Otter POST Jul–Aug 08	189	23–40	8.4	13.8
C-130 GOTEX Feb 04	859	24–49	15.8	27.1
Electra TOGA-COARE Nov 92–Feb 93	938	26–48	3.9	9.4

We also use raw data collected by the Naval Postgraduate School's Center for Interdisciplinary Remotely-Piloted Aircraft Studies (CIRPAS) Twin Otter aircraft in five experiments: 1) outside Monterey Bay off the coast of California in August 2007 during the Cloud-Aerosol Research in the Marine Atmosphere IV experiment (CARMA IV); 2) outside Monterey Bay (Monterey) during April 2008 (Khelif et al. 1999); 3) the Rough Evaporation Duct experiment (RED) to the east (windward side) of Oahu in the Hawaiian Islands during August–September of 2001 (Anderson et al. 2004); 4) the Marine Atmospheric Boundary Layer Energy Budget (MABLEB) experiment during April 2007; and 5) the Physics Of Stratocumulus Top during July–August 2008 (POST).

We also use raw data collected by the National Center for Atmospheric Research (NCAR) C-130 Hercules aircraft in the Gulf Of Tehuantepec (GOTEX) on the Pacific coast of the Isthmus of Tehuantepec, Mexico, in February 2004 (Raga and Abarca 2007), and raw data collected by the NCAR Electra aircraft in TOGA COARE in the Pacific warm pool during November 1992 to February 1993 (Vickers and Esbensen 1998).

3. Methods

a. Reduction to 10-m neutral

To compare measurements taken at different levels above the surface in different boundary layer stabilities and to compare to other studies, we employ standard Monin–Obukhov similarity theory and prescribed stability functions to reduce the data to a standard height of 10 m and neutral conditions. The 10-m neutral wind speed is computed as (Andreas et al. 2012)

$$U_{\mathrm{N10}} = U - (u_*/\kappa)\ln(z/10) + (u_*/\kappa)\psi_m, \qquad (1)$$

where U is the observed vector-averaged wind speed at height z,

$$U = (\overline{u}^2 + \overline{v}^2)^{1/2}, \qquad (2)$$

and ψ_m is a function of z/L where L is the Obukhov length scale. The overbar denotes averaging over 4-km flight segments and κ is the von Kármán constant (0.4). The scalar average wind speed at height z is given by

$$S = \overline{(u^2 + v^2)^{1/2}}, \qquad (3)$$

and the 10-m neutral scalar wind is given by

$$S_{\mathrm{N10}} = S - (u_*/\kappa)\ln(z/10) + (u_*/\kappa)\psi_m. \qquad (4)$$

Scalar averaging the wind speed violates Reynolds averaging for the vector equations of motion; however, we include it here as an alternative velocity scale because some studies employ an additional velocity scale to augment the vector averaged wind in weak wind conditions (e.g., Fairall et al. 1996).

The friction velocity is given by

$$u_* = (\overline{w'u'}^2 + \overline{w'v'}^2)^{1/4}, \qquad (5)$$

where u, v, and w are the fast-response (20–50 Hz depending on the experiment) along-wind, crosswind, and vertical components of the wind, and primes denote deviations from the 4-km mean. The friction velocity excluding the crosswind component of the stress is

$$ul_* = (\overline{w'u'}^2)^{1/4}. \qquad (6)$$

Note that $\overline{v}$ is zero by definition but that $\overline{w'v'}$ is not necessarily zero because of directional shear of the mean wind. In addition, the stress and wind direction can theoretically be independent of height but not aligned.

The quantity ψ_m is the integrated stability function given by

$$\psi_m(\zeta) = 2\ln\left(\frac{1+x}{2}\right) + \ln\left(\frac{1+x^2}{2}\right) - 2\tan^{-1}(x) + \pi/2; \quad \zeta < 0, \quad \text{and} \qquad (7)$$

$$\psi_m(\zeta) = -a_2\zeta; \quad \zeta > 0, \qquad (8)$$

where $x = (1 - a_1\zeta)^{1/4}$, $a_1 = 16$, $a_2 = 5$, and $\zeta = z/L$ (Businger 1966; Businger et al. 1971; Paulson 1970; Dyer 1974; Högström 1988). The stability function is zero for neutral conditions. The L is defined as

$$L \equiv \frac{-u_*^3}{(\kappa g/\theta_v)(\overline{w'\theta'} + 0.61\theta\overline{w'q'})}, \qquad (9)$$

where θ_v is the virtual potential temperature, θ is the potential temperature, g is the acceleration of gravity, and q is the specific humidity. The 10-m neutral drag coefficient is then computed as

$$C_{\mathrm{DN10}} = u_*^2 U_{\mathrm{N10}}^{-2}. \qquad (10)$$

Some studies apply an adjustment to the flux to account for possible (but unknown) significant vertical flux divergence between the aircraft altitude and the surface. We have found that extrapolation of the flux to the surface is subject to much uncertainty and is not significant except in shallow stable boundary layers when z/L exceeds about 0.1 for low-level aircraft data collected at 20–40-m altitude. In this study, less than 10% of the 4-km data segments have z/L greater than 0.1 after data screening is applied (see section below). As also noted below, flux segments within 8 km of shore are always excluded from our analysis because of the likelihood of shallow stable internal boundary layers near the coast with warm offshore flow. As a test, we evaluated the boundary layer depth formulation suggested by Donelan (1990) based on the friction velocity, the Coriolis parameter, and a dimensionless coefficient, together with an assumed linear decrease of the flux with height. This method increases the flux estimates by 5%–10% for those segments where z/L exceeds 0.1, and by less than a few percent for unstable and neutral conditions. Given the large uncertainty in predicting stable boundary layer depth from the friction velocity at a single height (Vickers and Mahrt 2004), and the small overall impact on our basic results, we choose to not make any adjustment.

b. Bin averaging

Our main objective here is to study how sensitive C_{DN10} is to the analysis method. As such, we will compute the 10-m neutral drag coefficient using different methods and bin average as a function of the 10-m

neutral wind speed in different ways to explore the sensitivity to the analysis method. The six different bin-averaging methods (denoted A-F) include

$$C_{\mathrm{DA}} = 10^3[u_*^2 U_{\mathrm{N10}}^{-2}], \tag{11}$$

$$C_{\mathrm{DB}} = 10^3[u_*^2 S_{\mathrm{N10}}^{-2}], \tag{12}$$

$$C_{\mathrm{DC}} = 10^3[ul_*^2 U_{\mathrm{N10}}^{-2}], \tag{13}$$

$$C_{\mathrm{DD}} = 10^3[u_*]^2[U_{\mathrm{N10}}]^{-2}, \tag{14}$$

$$C_{\mathrm{DE}} = 10^3([\overline{w'u'}]^2 + [\overline{w'v'}]^2)^{1/2}[U_{\mathrm{N10}}]^{-2}, \quad \text{and} \tag{15}$$

$$C_{\mathrm{DF}} = 10^3([\overline{w'u'}]^2)^{1/2}[U_{\mathrm{N10}}]^{-2}, \tag{16}$$

where the square brackets ([·]) denote bin averaging for bins of U_{N10}. The factor of 10^3 in Eqs. (11)–(16) is included to make values of the drag coefficient order one. All estimates of C_{DN10} are positive because they are based on the magnitude of the flux.

The methods include bin averaging the drag coefficient (Eq. 11), using the scalar average wind instead of the vector average (Eq. 12), excluding the crosswind component of the stress (Eq. 13), bin-averaging u_* and U_{N10} (Eq. 14), bin averaging the stress components (Eq. 15), and bin averaging the along-wind component of the stress and excluding the crosswind component (Eq. 16).

Note that interpreting the bin averages as depending only on wind speed assumes that the only important difference between bins is the 10-m neutral wind. This assumption requires that Monin–Obukhov similarity holds and that the stability functions are correct. Bin averaging reduces random errors but also reduces the influence of real physics of varying sign. For example, wave state might strongly influence the weak wind stress most of the time, but wave state modification may be of either sign. As a result, the influence of wave state is reduced by the bin averaging. In this sense, bin averaging is not an ensemble average over a uniform population.

c. Data screening

The aircraft data are first screened to identify straight, low-level flight segments suitable for computing turbulence fluxes. Conditions are imposed based on changes in aircraft heading, pitch, roll, and altitude. The aircraft altitude is required to be less than 50 m, and flights located within 8 km of land are excluded. The fast-response measurements of the wind, temperature, and humidity are screened using quality control software to identify and remove data with suspected instrumental error. After imposing these criteria, there are a total of 6125 4-km flight segments in the aircraft dataset suitable for computing air-sea fluxes (Table 1).

Following tradition and expectations, we assume that including the stability functions generally does more good than harm; however, calculating the 10-m neutral wind can sometimes lead to unrealistically large differences between U and U_{N10}. Such cases are not plausible and are associated with failure of similarity theory, incorrect stability functions, measurement error, or measurement uncertainty. Even when reduction of the wind to 10-m neutral does not lead to absurd results, such as negative U_{N10}, it can lead to suspiciously large corrections. As a result, we flag data points where the ratio U_{N10} divided by U is less than 0.8 or greater than 1.2. These outliers are associated with relatively strong stability effects where the magnitude of z/L approaches unity for the higher altitude flight segments. The cases of negative U_{N10} all occur in strongly stable conditions ($z/L > 1$) where the stability function decreases the mean wind speed with decreasing height at a rate much faster than is realistic.

In addition, we flag data points where C_{DN10} exceeds 100. Such values for the sea surface drag coefficient are at least an order of magnitude larger than thought to be plausible. These are weak wind cases with significant stability, including both stable and unstable conditions. After all screening has been applied, 5800 4-km data points remain for further analysis (95% of the total possible).

The impact on the drag coefficient of the reduction to 10-m neutral stability using Monin–Obukhov similarity theory and the prescribed stability functions is shown in Fig. 2. The ratio of C_D to C_{DN10} decreases continuously with increasing atmospheric stability. The ratio in neutral conditions (0.85, Fig. 2) represents the height correction for a log profile. That is, for neutral conditions, C_{DN10} is greater than C_D because the wind speed at aircraft altitude is greater than the wind speed at 10 m, while the variation of the momentum flux with height is assumed to be small. The neutral equivalent drag coefficient decreases with height in the surface layer.

d. Published formulations

Our estimates of C_{DN10} will be compared to the widely used Charnock plus smooth flow formulation of the aerodynamic roughness length,

$$z_0 = \alpha u_*^2/g + 0.11\nu/u_*, \tag{17}$$

following Charnock (1955), Smith (1988), Fairall et al. (1996), and others, where α is the Charnock coefficient

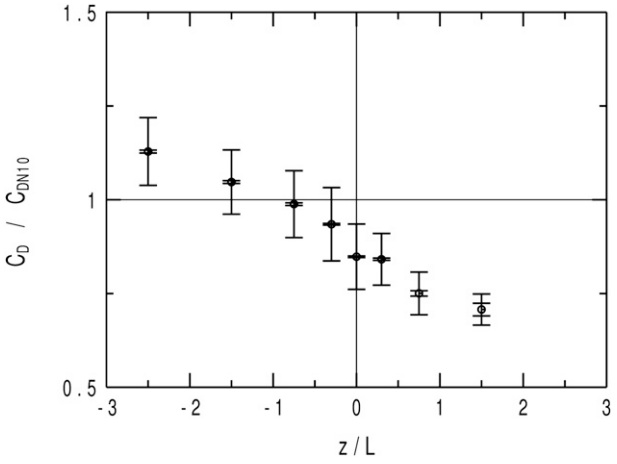

FIG. 2. The ratio C_D divided by C_{DN10}, bin averaged by the stability parameter z/L. The inner error bars denote ± 1 standard error; and the outer error bars, $\pm$ one standard deviation. C_D is defined as u_*^2 divided by U^2.

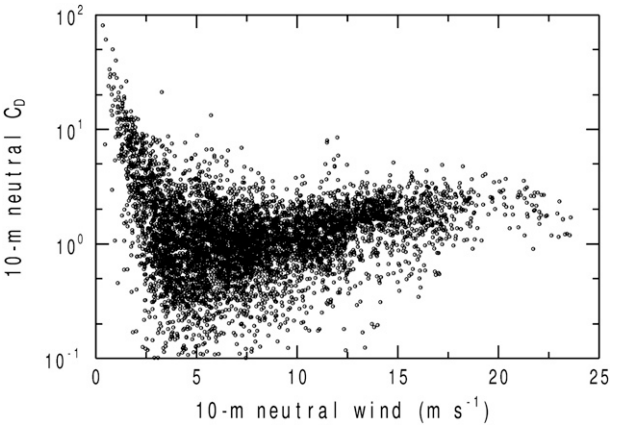

FIG. 3. Individual 4-km values of the 10-m neutral drag coefficient as a function of the 10-m neutral wind speed. There are 5800 data points.

($\alpha = 0.011$), and ν is the kinematic viscosity of dry air. The first term on the right-hand side of Eq. (17) states that the aerodynamic roughness of the sea surface is proportional to the downward turbulence momentum transport from the atmosphere. The second term on the right-hand side of Eq. (17) is the aerodynamically smooth flow (viscous) term (Kondo 1975; Liu et al. 1979), which is important in the formulation only in weak winds. The roughness length and the 10-m neutral drag coefficient are related as

$$C_{\mathrm{DN10}} = \left[\frac{\kappa}{\ln(10/z_0)}\right]^2. \tag{18}$$

Numerous investigators have related variations in α (the nondimensional roughness) to variations in wave state (phase speed, wavelength) to include larger wind stress observed over young growing waves and smaller wind stress observed over older, faster moving waves (Donelan 1990; Smith et al. 1992; Drennan et al. 2003). Here we use the constant value of α, without wave-state effects, from the TOGA COARE bulk flux algorithm.

We also compare to a consensus formulation published by Garratt (1977) based on an extensive literature review,

$$C_{\mathrm{DN10}} = 0.75 + 0.067 U_{\mathrm{N10}}, \tag{19}$$

for U_{N10} between 4 and 21 m s^{-1}. The linear form in Eq. (19) is a close approximation to the Charnock formulation with $\alpha = 0.0144$. The wind speed dependence of C_{DN10} is also compared to the Large and Pond (1981) and Andreas et al. (2012) formulations.

4. Results

Individual 4-km estimates of the 10-m neutral drag coefficient as a function of the 10-m neutral wind are shown in Fig. 3. Both quantities (U_{N10} and C_{DN10}) are derived from the observations, similarity theory, and the prescribed stability functions as described in the previous section. The dominant features are the large scatter in C_{DN10} (note the log scale in Fig. 3) and an apparent local minimum in C_{DN10} for wind speeds around 4 m s^{-1}.

a. Sensitivity to calculation method

The sensitivity of the relationship between U_{N10} and C_{DN10} to the six different calculation methods [Eqs. (11)–(16)] is shown in Fig. 4. There is only a small reduction in C_{DN10} when we replace the vector average wind with the scalar average in weak wind conditions (cf. weak winds in Figs. 4a,b), indicating that changes in wind direction on scales less than 4 km are generally small. Excluding the crosswind component of the stress reduces C_{DN10} in weak winds, suggesting a systematic crosswind stress that survives the bin averaging (cf. weak winds in Figs. 4a,c). Bin-averaging u_* and U_{N10} and then taking the ratio, compared to averaging the ratio, reduces C_{DN10} in weak winds (cf. Figs. 4a,d).

Bin averaging the stress components strongly reduces C_{DN10} in weak winds (cf. Figs. 4a,e). This is due to conversion of random flux sampling errors into systematic flux errors when bin-averaging C_{DN10}. That is, very small values of $\overline{w'u'}$ in weak winds are dominated by random sampling error that can even change the sign of the flux component. Therefore, averaging the components rather the square of the components leads to a smaller flux. We note that true ensemble averaging and therefore quantification of purely random sampling

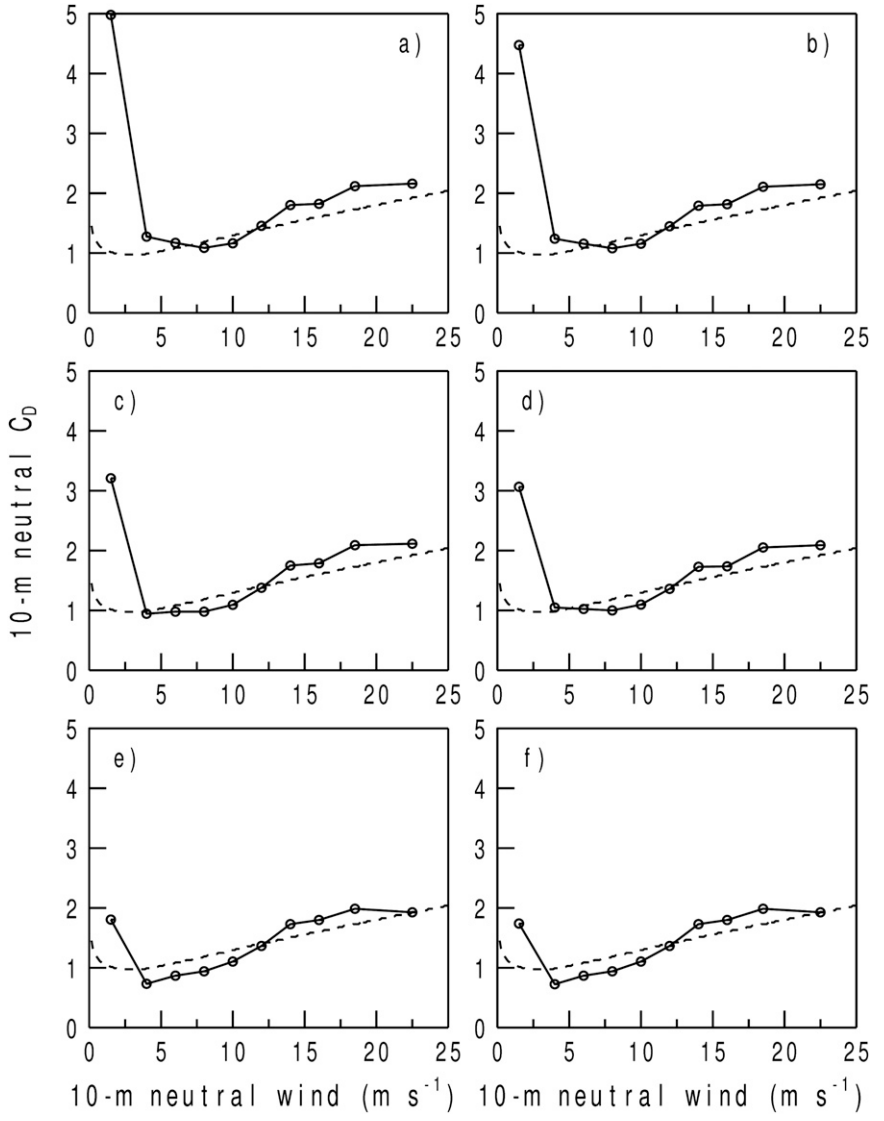

FIG. 4. The 10-m neutral drag coefficient as a function of the 10-m neutral wind for six different computation methods: (a) Eq. (11), (b) Eq. (12), (c) Eq. (13), (d) Eq. (14), (e) Eq. (15), and (f) Eq. (16). The dashed curve (same in each panel) is the Charnock plus smooth flow relationship with $\alpha = 0.011$. There are 10 wind speed bins: 0–3, 3–5, 5–7, 7–9, 9–11, 11–13, 13–15, 15–17, 17–20, and 20–25 m s^{-1}.

errors is not obtainable. Excluding the crosswind stress when bin-averaging the stress components has little effect on C_{DN10} (cf. Figs. 4e,f).

This analysis shows that calculating C_{DN10} in weak winds is not well posed because the result is strongly sensitive to the choice of analysis method. In the literature, it is not always clear what specific analysis method was used. Many studies use only the along-wind component of the stress, and some studies average ratios instead of taking the ratio of averages. Possibly to avoid these problems, studies often do not show estimates of the drag coefficient for weak winds (Fig. 1). In moderate to strong winds, where the relative random flux sampling error is less owing to much larger values of the wind stress, C_{DN10} is not as sensitive to the analysis method. Analysis problems for C_{DN10} in weak winds were also pointed out by Mahrt et al. (1996) using a tower dataset.

b. Wind regimes

The wind speed dependence of C_{DN10}, excluding the weak-wind regime, is shown in Fig. 5, where u_* is computed using Eq. (5), the wind with Eq. (2), and the bin

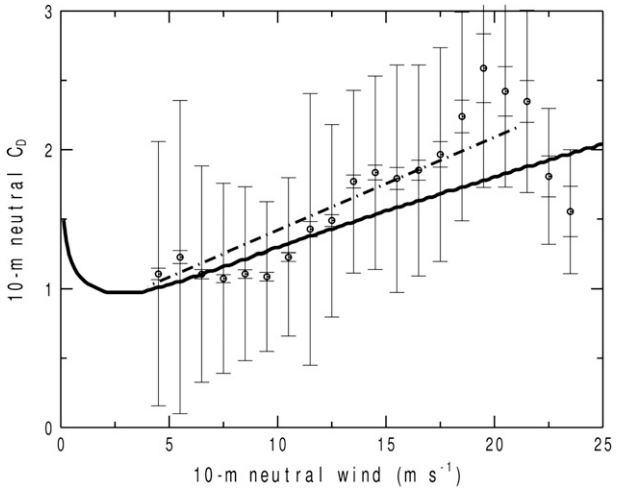

FIG. 5. The 10-m neutral drag coefficient bin averaged by the 10-m neutral wind for winds > 4 m s^{-1}. The wind speed bins are 1 m s^{-1} wide from 4 to 24 m s^{-1}. The inner error bars denote ± 1 standard error; and the outer error bars, $\pm$ one standard deviation (see also Table 2). The heavy curve is the Charnock plus smooth flow relationship with $\alpha = 0.011$, and the dash-dot straight line is from Garratt's (1977) review paper (Eq. 19).

averaging using Eq. (11). The values of C_{DN10} for all wind speeds are tabulated in Table 2. Some of the scatter in Fig. 5 may be due to systematic differences in wave state and possibly instrumentation among the different datasets. The generally lower values of C_{DN10} found for CARMA IV for U_{N10} between 8 and 15 m s^{-1} (Fig. 6) are associated with stable atmospheric conditions. The largest values of C_{DN10} for winds above 12 m s^{-1} are found for GOTEX (Fig. 6). The enhanced drag for GOTEX may be related to wave state and fetch limited off-shore flow. The largest values of C_{DN10} for U_{N10} between 4 and 6 m s^{-1} are found for Long-EZ SHOWEX November 97.

Four wind speed regimes are evident from the combined dataset.

- For $U_{N10} < 4$ m s^{-1}, calculation of C_{DN10} is not well posed.
- For 4 m s^{-1} $< U_{N10} <$ 10 m s^{-1}, C_{DN10} is nearly constant with wind speed and is 1.12. Large and Pond (1981) found the same result where C_{DN10} was constant (1.13) for U_{N10} between 4 m s^{-1} and 10 m s^{-1} (Fig. 1).
- For 10 m s^{-1} $< U_{N10} <$ 20 m s^{-1}, C_{DN10} increases with wind speed likely because of the onset and continued development of wave breaking, which enhances the drag (Banner and Melville 1976; Melville 1977; Banner 1990). According to the analysis of Andreas et al. (2012), the transition at about 10 m s^{-1} is the transition to fully aerodynamically rough flow. In this wind regime, C_{DN10} is similar to that reported by Geernaert et al. (1986). The rate of increase in C_{DN10} with increasing wind speed is the same as found by Smith et al. (1992) based on data from the Humidity Exchange Over the Sea (HEXOS).
- For winds exceeding 20 m s^{-1}, C_{DN10} steadily decreases with increasing wind speed based on GOTEX data alone. Note, however, there are few data in these bins (Table 2).

TABLE 2. The 10-m neutral drag coefficient bin-averaged by the 10-m neutral wind speed using the method in Eq. (11). Results for $U_{N10} < 4$ m s^{-1} are sensitive to the calculation method and thus not well posed. The N is the number of samples in each bin. The drag coefficient has been multiplied by 10^3 to make it of order one. Note the decrease in C_{DN10} with increasing U_{N10} for $U_{N10} >$ 20 m s^{-1}.

U_{N10} (m s^{-1})	Mean	Std error	Std dev	N
0–1	25.3	4.34	19.8	21
1–2	7.49	0.362	5.01	191
2–3	2.63	0.114	2.16	387
3–4	1.43	0.063	1.52	573
4–5	1.11	0.042	0.95	525
5–6	1.23	0.046	1.13	609
6–7	1.11	0.034	0.78	535
7–8	1.07	0.029	0.68	559
8–9	1.11	0.031	0.62	407
9–10	1.08	0.031	0.54	303
10–11	1.23	0.030	0.57	343
11–12	1.43	0.055	0.98	313
12–13	1.49	0.042	0.69	267
13–14	1.77	0.047	0.66	199
14–15	1.84	0.053	0.70	174
15–16	1.79	0.079	0.82	108
16–17	1.85	0.072	0.76	112
17–18	1.97	0.092	0.77	70
18–19	2.24	0.120	0.75	41
19–20	2.59	0.248	0.86	12
20–21	2.42	0.178	0.69	15
21–22	2.35	0.151	0.66	19
22–23	1.81	0.148	0.49	11
23–24	1.55	0.182	0.45	6

GOTEX is the only dataset with $U_{N10} > 20$ m s^{-1} and is the only dataset that shows a steady decrease in C_{DN10} with increasing wind speed for strong winds (Fig. 6). This result for GOTEX does not change if we increase the averaging length scale from 4 to 8 km, which could potentially capture more flux on larger scales leading to a larger u_* and larger C_{DN10}. The GOTEX result may not be representative of other regions as the site was chosen specifically to sample strong offshore gap winds; however, the sampling problems are somewhat mitigated because the low-level aircraft flight tracks used here are perpendicular to the off-shore jet and thus sampled the crosswind variability of the stress and the wind speed.

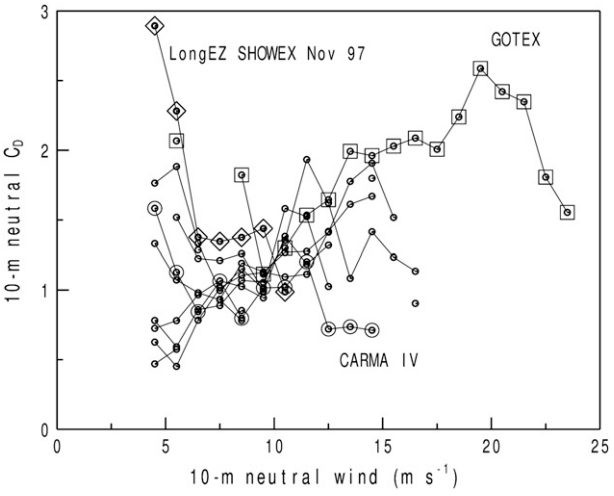

FIG. 6. The 10-m neutral drag coefficient bin averaged by the 10-m neutral wind for winds > 4 m s^{-1}. Bins are 1 m s^{-1} wide from 4 to 24 m s^{-1}. Multiple values of C_{DN10} for the same wind speed denote different datasets. A minimum of six observations is required per dataset per bin. Data points with a circle are from CARMA IV; a square from GOTEX; and a diamond from SHOWEX November 97.

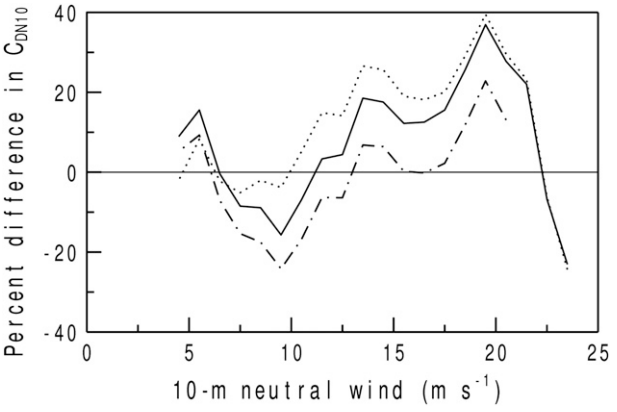

FIG. 7. The percent difference in the 10-m neutral drag coefficient for this study minus Charnock (solid), this study minus Garratt (1977) (dash-dot), and this study minus Large and Pond (1981) (dotted) bin-averaged by the 10-m neutral wind speed.

While the GOTEX data support a decrease in C_{DN10} for winds in excess of 20 m s^{-1}, previous studies have proposed a higher wind speed threshold. Jarosz et al. (2007) reported a maximum in C_{DN10} for U_{N10} of 35 m s^{-1}, and Powell et al. (2003) found a maximum for U_{N10} of 40 m s^{-1}. We note that the Jarosz et al. (2007) and Powell et al. (2003) estimates of C_{DN10} are not based on eddy-covariance measurements. French et al. (2007) found a leveling off followed by a slight decrease in C_{DN10} with increasing U_{N10} for U_{N10} greater than about 20 m s^{-1}. Their estimates for C_{DN10}, based on eddy-covariance measurements, are very close to the Charnock formulation for U_{N10} between 21 and 23 m s^{-1}, higher than Charnock for U_{N10} from 16 to 21 m s^{-1}, and significantly lower than Charnock for their strongest wind speeds from 25 to 29 m s^{-1}. Unfortunately, the number of samples and the range of observed wind speeds in CBLAST Hurricane is small. The fluxes were measured at altitudes between 70 and 383 m with a median level of 193 m. French et al. (2007) applied a correction to account for the decrease of the flux with height.

Our results can be summarized by a simple piecewise linear formulation that includes the constant C_{DN10} regime and the transition to increasing drag at U_{N10} equal to 10 m s^{-1}. In the formulation, C_{DN10} is constant at 1.12 for winds between 4 and 10 m s^{-1} and then increases linearly with a slope of 0.12 for winds between 10 and 21 m s^{-1}.

c. *Other formulations*

The differences between C_{DN10} from this study and three published formulations are summarized in Figs. 7 and 8. Other than the largest differences of nearly 40% found for the Charnock and Large and Pond formulations for U_{N10} near 20 m s^{-1}, the differences are generally within ±25% (Fig. 7). The Charnock form with $\alpha = 0.011$ and the Large and Pond formulation both substantially underpredict C_{DN10} for U_{N10} between 14

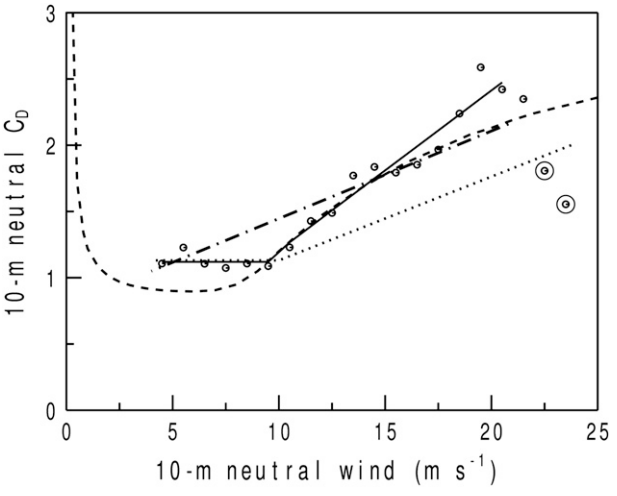

FIG. 8. A simple model formulation (two straight lines) that describes the current data (20 dots). The two strongest wind speed data points (with circles) are excluded from the model because more strong wind data are needed to test this result. Weak winds < 4 m s^{-1} are excluded because the result is strongly sensitive to the choice of analysis method. Previously published formulations include Andreas et al. (2012) (dashed), Large and Pond (1981) (dotted), and Garratt (1977) (dash-dot).

and 21 m s^{-1}. In this wind speed range, Eq. (19) proposed by Garratt (1977) is closer to the current observations than is the Charnock or Large and Pond formulations.

The dashed curve in Fig. 8 is from Andreas et al. (2012) and is based on the same aircraft datasets used in this study with the addition of processed (precalculated fluxes) datasets collected on towers, ships, and other aircraft. In addition, the data screening procedures used were different from this study. More importantly, Andreas et al. (2012) employed a different approach in which u_* was modeled as a linear function of U_{N10}. They extended the model to weak winds using a smooth flow representation and extrapolated their estimate of C_{DN10} to stronger wind speeds. The Andreas et al. (2012) model agrees with the current data for U_{N10} between 10 and 15 m s^{-1}, but otherwise yields a smaller drag coefficient than that suggested by the current study and the traditional approach of modeling C_{DN10} in terms of U_{N10}. In this study, we are evaluating the traditional approach of modeling C_{DN10} in terms of U_{N10}, not necessarily recommending it.

While the Large and Pond formulation fits the data well for U_{N10} between 4 and 10 m s^{-1}, where C_{DN10} is constant, it substantially underpredicts the rate of increase in C_{DN10} for U_{N10} between 10 and 23 m s^{-1} (Fig. 8). The Garratt form generally gives larger drag for U_{N10} less than 15 m s^{-1} and smaller drag for U_{N10} between 15 and 21 m s^{-1} compared to the current data. The linear rate of increase in C_{DN10} found here for U_{N10} between 10 and 20 m s^{-1} is the same as that reported by Smith et al. (1992) based on the HEXOS results (Fig. 1). However, while the slopes are the same, the HEXOS results suggest a larger C_{DN10} than the current study.

5. Conclusions

A large aircraft dataset including 11 different experiments with four different aircraft was used to study the dependence of the neutral equivalent drag coefficient on wind speed in the context of Monin–Obukhov similarity theory. Our main objective was to investigate how sensitive C_{DN10} is to the method of analysis. Therefore, we tested six different calculation methods, with the main finding being that bin averaging the 10-m neutral drag coefficient in weak winds leads to overestimates of the drag coefficient due to conversion of random flux sampling errors into systematic errors. Calculating the drag coefficient is ill-posed in weak winds because the results depend on the method of analysis. This problem becomes less important for stronger winds exceeding about 4 m s^{-1}.

Four distinct wind regimes were identified: weak winds where calculating C_{DN10} is not well posed, moderate winds (4 to 10 m s^{-1}) where C_{DN10} is a constant, strong winds (10 to 20 m s^{-1}) where C_{DN10} increases linearly with increasing wind speed, and very strong winds exceeding 20 m s^{-1} where C_{DN10} steadily decreases with increasing wind speed; although more strong wind data are needed to confirm this result. Differences between our estimates of C_{DN10} and other published formulations are generally within ±25% depending on wind speed.

The observations here are summarized by a simple piecewise linear formulation of the wind speed dependence of C_{DN10} for 10-m neutral winds between 4 and 21 m s^{-1}. The data suggest a critical 10-m neutral wind speed of about 10 m s^{-1} associated with the onset of enhanced drag likely owing to wave breaking and the transition to fully aerodynamically rough flow. The formulation is incomplete because it is not valid for weak winds or very strong winds.

Acknowledgments. We thank the many dedicated scientists who collected and made available the fast-response aircraft data. The U.S. Office of Naval Research supported this work with Award N00014-11-1-0073 to NorthWest Research Associates. ONR also supported ELA through the National Ocean Partnership Program with Award N00014-10-1-0154 to the University of Rhode Island, for whom he is a contractor.

REFERENCES

Anderson, K., and Coauthors, 2004: The RED experiment: An assessment of boundary layer effects in a tradewinds regime on microwave and infrared propagation over the sea. *Mon. Wea. Rev.,* **132,** 1355–1365.

Andreas, E. L, L. Mahrt, and D. Vickers, 2012: A new drag relation for aerodynamically rough flow over the ocean. *J. Atmos. Sci.,* **69,** 2520–2537.

Banner, M. L., 1990: The influence of wave breaking on the surface pressure distribution in wind-wave interactions. *J. Fluid Mech.,* **211,** 463–495.

——, and W. K. Melville, 1976: On the separation of air flow over water waves. *J. Fluid Mech.,* **77,** 825–842.

Businger, J. A., 1966: Transfer of momentum and heat in the planetary boundary layer. *Proc. Symp. Arctic Heat Budget and Atmospheric Circulation,* Santa Monica, CA, the RAND Corporation, 305–331.

——, J. C. Wyngaard, Y. Izumi, and E. F. Bradley, 1971: Flux–profile relationships in the atmospheric surface layer. *J. Atmos. Sci.,* **28,** 181–189.

Charnock, H., 1955: Wind stress over a water surface. *Quart. J. Roy. Meteor. Soc.,* **81,** 639–640.

Donelan, M. A., 1982: The dependence of the aerodynamic drag coefficient on wave parameters. Preprints, *First Int. Conf. on Meteorology and Air–Sea Interaction of the Coastal Zone,* Boston, MA, Amer. Meteor. Soc., 381–387.

——, 1990: Air-sea interaction. *The Sea,* B. LeMehaute and D. M. Hanes, Eds. *Ocean Engineering Science,* Vol. 9, John Wiley and Sons, 239–292.

Drennan, W. M., H. Graber, D. Hauser, and C. Quentin, 2003: On the wave age dependence of wind stress over pure wind seas. *J. Geophys. Res.,* **108,** 8062.

Dyer, A. J., 1974: A review of flux-profile relationships. *Bound.-Layer Meteor.,* **7,** 363–372.

Edson, J. B., and Coauthors, 2007: The coupled boundary layers and air–sea transfer experiment in low winds. *Bull. Amer. Meteor. Soc.,* **88,** 341–356.

Fairall, C. W., E. F. Bradley, D. P. Rogers, J. B. Edson, and G. S. Young, 1996: Bulk parameterization of air–sea fluxes for Tropical Ocean–Global Atmosphere Coupled-Ocean Atmosphere Response Experiment. *J. Geophys. Res.,* **101,** 3747–3764.

——, ——, J. E. Hare, A. A. Grachev, and J. B. Edson, 2003: Bulk parameterization of air–sea fluxes: Updates and verification for the COARE algorithm. *J. Climate,* **16,** 571–591.

French, J. R., W. M. Drennan, J. A. Zhang, and P. G. Black, 2007: Turbulent fluxes in the hurricane boundary layer. Part I: Momentum flux. *J. Atmos. Sci.,* **64,** 1089–1102.

Garratt, J. R., 1977: Review of drag coefficients over oceans and continents. *Mon. Wea. Rev.,* **105,** 915–929.

Geernaert, G. L., K. B. Katsaros, and K. Richter, 1986: Variation of the drag coefficient and its dependence on sea state. *J. Geophys. Res.,* **91,** 7667–7679.

Grachev, A. A., C. W. Fairall, J. E. Hare, J. B. Edson, and S. D. Miller, 2003: Wind stress vector over ocean waves. *J. Phys. Oceanogr.,* **33,** 2408–2429.

Högström, U., 1988: Non-dimensional wind and temperature profiles in the atmospheric surface layer: A re-evaluation. *Bound.-Layer Meteor.,* **42,** 55–78.

Jarosz, E., D. A. Mitchell, D. W. Wang, and W. J. Teagure, 2007: Bottom-up determination of air-sea momentum exchange under a major tropical cyclone. *Science,* **23,** 1707–1709.

Khelif, D., S. P. Burns, and C. A. Friehe, 1999: Improved wind measurements on research aircraft. *J. Atmos. Oceanic Technol.,* **16,** 860–875.

Kondo, J., 1975: Air-sea bulk transfer coefficients in diabatic conditions. *Bound.-Layer Meteor.,* **9,** 91–112.

Large, W. G., and S. Pond, 1981: Open ocean momentum flux measurements in moderate to strong winds. *J. Phys. Oceanogr.,* **11,** 324–336.

Liu, W. T., K. B. Katsaros, and J. A. Businger, 1979: Bulk parameterization of the air-sea exchange of heat and water vapor including the molecular constraints at the interface. *J. Atmos. Sci.,* **36,** 1722–1735.

Mahrt, L., D. Vickers, J. Howell, J. Højstrup, J. A. Wilczak, J. Edson, and J. Hare, 1996: Sea surface drag coefficients in RASEX. *J. Geophys. Res.,* **101,** 14 327–14 335.

Melville, W. K., 1977: Wind stress and roughness length over breaking waves. *J. Phys. Oceanogr.,* **7,** 702–710.

Paulson, C. A., 1970: The mathematical representation of wind speed and temperature profiles in the unstable atmospheric surface layer. *J. Appl. Meteor.,* **9,** 857–861.

Powell, M. D., P. J. Vickery, and A. Reinhold, 2003: Reduced drag coefficient for high wind speeds in tropical cyclones. *Nature,* **422,** 279–283.

Raga, G., and S. Abarca, 2007: On the parameterization of turbulent fluxes over the tropical eastern Pacific. *Amer. Chem. Phys.,* **7,** 635–643.

Rieder, K. F., J. A. Smith, and R. A. Weller, 1994: Observed directional characteristics of the wind, wind stress and surface waves on the open ocean. *J. Geophys. Res.,* **22** (C11), 589–596.

Sheppard, P. A., D. T. Tribble, and J. R. Garratt, 1972: Studies of turbulence in the surface layer over water (Lough Neagh), Part 1. Instrumentation, programme, profiles. *Quart. J. Roy. Meteor. Soc.,* **98,** 627–641.

Smith, S. D., 1980: Wind stress and heat flux over the ocean in gale force winds. *J. Phys. Oceanogr.,* **10,** 709–726.

——, 1988: Coefficients for sea surface wind stress, heat flux, and wind profiles as a function of wind speed and temperature. *J. Geophys. Res.,* **93** (C12), 15 467–15 472.

——, and E. G. Banke, 1975: Variation of the sea surface drag coefficient with wind speed. *Quart. J. Roy. Meteor. Soc.,* **101,** 665–673.

——, and Coauthors, 1992: Sea surface wind stress and drag coefficients: The HEXOS results. *Bound.-Layer Meteor.,* **60,** 109–142.

Sun, J., D. Vandemark, L. Mahrt, D. Vickers, T. Crawford, and C. Vogel, 2001: Momentum transfer over the coastal zone. *J. Geophys. Res.,* **106,** 12 437–12 448.

Vickers, D., and S. K. Esbensen, 1998: Subgrid surface fluxes in fair weather conditions during TOGA COARE: Observational estimates and parameterization. *Mon. Wea. Rev.,* **126,** 620–633.

——, and L. Mahrt, 2004: Evaluating formulations of stable boundary-layer height. *J. Appl. Meteor.,* **43,** 1736–1749.